Optimization of highly circularly polarized thermal radiation in α-MoO_3/β-Ga_2O_3 twisted layers

Marco Centini, Chiyu Yang, Maria Cristina Larciprete, Mauro Antezza, Zhuoming Zhang

Journal of Quantitative Spectroscopy & Radiative Transfer 323 (2024) 109051

Contents lists available at ScienceDirect

Journal of Quantitative Spectroscopy and Radiative Transfer

journal homepage: www.elsevier.com/locate/jqsrt

Optimization of highly circularly polarized thermal radiation in α-MoO_3/β-Ga_2O_3 twisted layers

Marco Centini [a,*], Chiyu Yang [b], Maria Cristina Larciprete [a], Mauro Antezza [c,d], Zhuomin M. Zhang [b]

[a] Sapienza University of Rome Department of Basic and Applied Sciences for Engineering, Via A. Scarpa 14, I-00161 Rome, Italy
[b] George W. Woodruff School of Mechanical Engineering, Georgia Institute of Technology, Atlanta, GA 30332, USA
[c] Laboratoire Charles Coulomb (L2C), UMR 5221 CNRS-Université de Montpellier, F- 34095, Montpellier, France
[d] Institut Universitaire de France, 1 rue Descartes, F-75231 Paris Cedex 05, France

ARTICLE INFO

Keywords:
Thermal radiation
Circular polarization
Infrared photonics
Optical anisotropic thin films

ABSTRACT

We investigate a bi-layer scheme for circularly polarized infrared thermal radiation. Our approach takes advantage of the strong anisotropy of low-symmetry materials such as β-Ga_2O_3 and α-MoO_3. We numerically report narrow-band, high degree of circular polarization (over 0.85), thermal radiation at two typical emission frequencies related to the excitation of β-Ga_2O_3 optical phonons. Optimization of the degree of circular polarization is achieved by a proper relative tilt of the crystal axes between the two layers. Our simple but effective scheme could set the basis for a new class of lithography-free thermal sources for IR bio-sensing.

1. Introduction

The development of miniaturized and integrable devices operating in the mid-infrared (mid-IR) relies on the availability of narrowband, highly directional, and polarization tunable sources. Indeed, several applications ranging from IR sensing [1,2] to biomedical diagnostics and target detecting [3,4] as well as for the realization of integrated IR photonics [5,6] require highly efficient, narrow-band, and polarization tunable mid-IR sources. An efficient but expensive option is represented by quantum cascade laser (QCL) IR sources. However, with the aim to achieve mass production of low-cost devices, a lot of research effort has been recently spent on the study of optimized and controllable thermal radiation sources. Thanks to the development of micro/nano technologies [7], several approaches to control and tailor the typically incoherent and broadband thermal radiation from heated bodies have been proposed and realized. The mechanism at the base of this tailored emission is the excitation of resonant states i.e. surface plasmon-(SP) or phonon-(SPh) polaritons, Bloch surface waves, magnetic polaritons, to name a few. Gratings [8], metamaterials [9,10], metasurfaces [11] and nanoantennae [12,13] have been successfully proposed to overcome the limits and enhance the performances of natural bulk materials. However, all these approaches rely on the use of lithographic techniques to artificially create absorption/emission resonances as well as a strong birefringent effective response. In particular, birefringence is necessary for polarization-sensitive applications.

An extreme form of birefringent behavior is called hyperbolicity and it is achieved when one diagonal element of the material dielectric tensor is negative, whilst the others are positive. Hyperbolic metamaterials obtained by periodic sub-wavelength patterned layered media have been extensively studied for photonics application [14-17] as well as for enhanced thermal radiation and nanoscale heat transfer [18,19]. However, it has been recently shown that hyperbolicity can be observed in natural materials, more specifically in van der Waals (vdW) materials IR [20]. Among vdW materials, hexagonal boron nitride hBN is one of the most investigated [21]. The hBN exhibits two different Restsrahlen bands (negative values of the real part of the permittivity) along either the in-plane or out-of-plane directions. The main limitation of hBN is the lack of in-plane anisotropy. In-plane anisotropy is required to distinguish and manipulate orthogonal polarization states of the electromagnetic field at normal incidence.

Among the vdW polar materials displaying in-plane anisotropy, molybdenum trioxide (α-MoO_3) has been the object of a conspicuous number of recent studies [22,23]. Its strong anisotropy, allowing in-plane and off-plane hyperbolicity, has been used to obtain mid-IR waveplates [24] and tunable [25] and broadband [26] absorption in the far-field. Concerning the excitation of surface waves, hyperbolic

* Corresponding author.
E-mail address: marco.centini@uniroma1.it (M. Centini).

https://doi.org/10.1016/j.jqsrt.2024.109051
Received 20 October 2023; Received in revised form 7 May 2024; Accepted 13 May 2024
Available online 22 May 2024

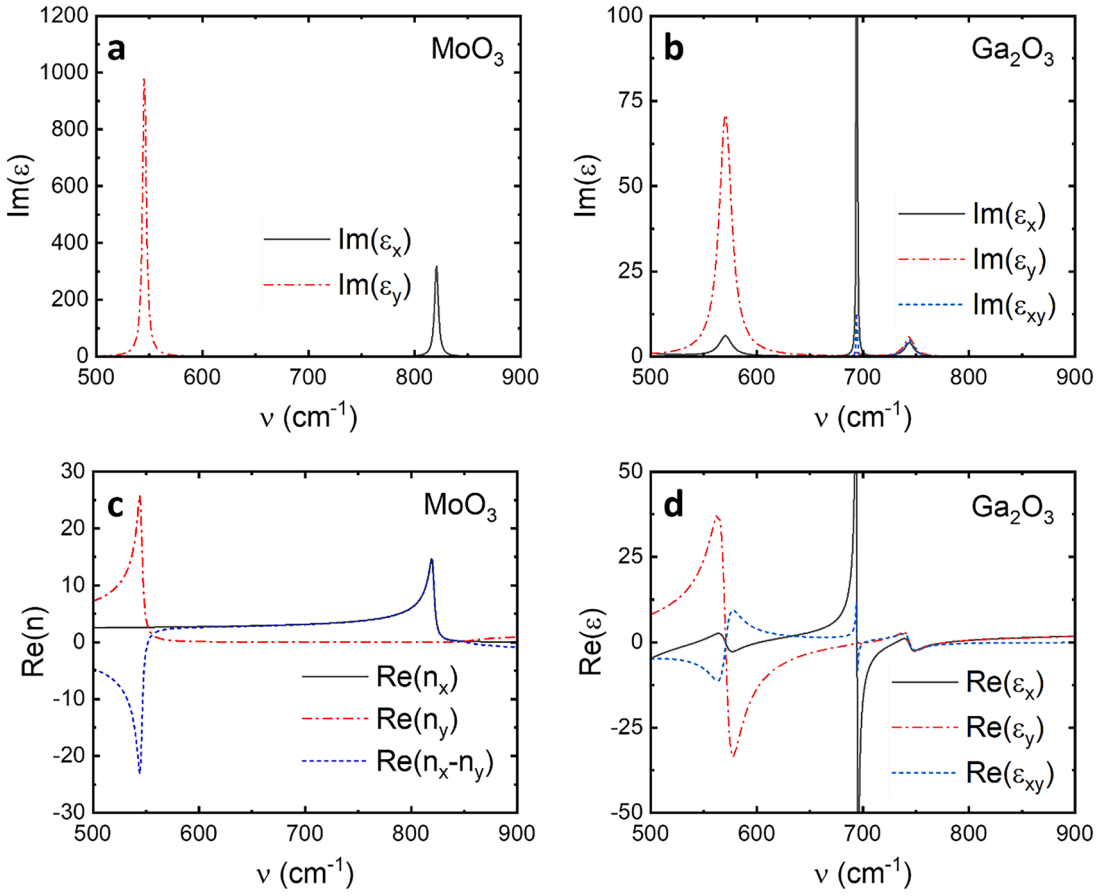

Fig. 1. Imaginary part of the in-plane components (*xx,xy,yy*) of the dielectric permittivity tensor of (a) MoO_3, (b) Ga_2O_3. Real part of the refractive indices along *x*- (n_x) and *y*- (n_y) directions and Δn for (c) MoO_3 and Real part of the relative permittivity for (d) Ga_2O_3.

phonon polaritons have recently been shown in α-MoO_3 flakes from 818 cm^{-1} to 974 cm^{-1} [23,27]. Furthermore, the excitation of SPh polaritons waves in twisted flakes of 2D α-MoO_3 has been proposed and experimentally verified [28]. Such control of SPh polaritons in twisted flakes has interesting applications for tunable near-field radiative heat transfer [29] by adjusting the tilt angle between the receiver and the emitter. It has been shown that twisted α-MoO_3 layers can exhibit circular dichroism [30,31] and can be used to generate spin thermal radiation [32]. However, using twisted structures of identical anisotropic materials to achieve spin thermal radiation has more restrictions on the materials. For this reason, α-MoO_3 was combined with an ideal quarter wavelength plate [33]. However, a tunable combination of two real anisotropic materials (i.e. controlling the tilt angle between them) could be adopted for practical applications and integrated thermal sources.

Low-symmetry materials have recently emerged as possible candidates for anisotropic optical applications [30]. Among them, β-Ga_2O_3 [34,35] has been used to experimentally demonstrate the excitation of shear phonon polaritons in the IR [36,37]. Moreover, this material perfectly matches the usable wavelength range of α-MoO_3. More specifically we will show that there are phonon resonances in the β-Ga_2O_3 which fall in an almost transparent but highly anisotropic band of the α-MoO_3. Thus, we propose a combination of two twisted layers obtained from these two materials.

Our calculations, based on a complete Stokes parameters analysis [38] of emitted radiation, show that it is possible to obtain circularly polarized thermal radiation in the mid-IR with a twisted bilayer system having about two microns of total thickness. As a starting point we study the emission properties and the birefringence behavior of single layers of α-MoO_3 and β-Ga_2O_3 on gold substrates. The choice of gold substrate allows for an almost one-sided emissivity as long as we can ignore thermal emission for the gold back face in the mid-IR. The relative permittivity of Au has been modeled from the data in [39]. After the choice of one of the two materials as the emitter, we add a properly tilted and sized layer of the other, acting as a quarter wave plate to obtain thermally radiated circularly polarized light.

2. Numerical methods

In order to quantitatively study the degree of polarization (DoP) and the degree of circular polarization (DoCP) of the thermal radiation polarization properties can be characterized by Stokes parameters. For reciprocal materials, the Stokes parameters can be expressed in terms of the polarized emissivities as [38,40]:

$$\begin{bmatrix} S_0 \\ S_1 \\ S_2 \\ S_3 \end{bmatrix} = \frac{S_{0,bb}(\omega, k_{\|})}{2} \begin{bmatrix} \epsilon_p + \epsilon_s \\ \epsilon_p - \epsilon_s \\ \epsilon_{45^\circ} - \epsilon_{135^\circ} \\ \epsilon_R - \epsilon_L \end{bmatrix} \tag{1}$$

where $k_{\|}$ is the wave vector projection onto the surface (*x*-*y*) plane, $S_{0,bb}$ is the emissivity of the black body, $\varepsilon_{p,s}$ are the *p*- and *s*- polarized relative emissivities, $\epsilon_{45^\circ,135^\circ}$ are the 45°- and 135°- polarized relative emissivities and $\varepsilon_{R,L}$ are the *right*- and *left*- circular polarized relative emissivities respectively. Limiting our discussion to reciprocal media at thermal equilibrium, polarized emissivities can be evaluated by calculating the polarized absorptivities α, according to Kirchhoff's law:

$$\epsilon_{p,s,45^\circ,135^\circ,R,L} = \alpha_{p,s,45^\circ,135^\circ,R,L} \tag{2}$$

Polarized absorptivities have been retrieved by evaluating $1 - R - T$ where R is reflectance and T is transmittance evaluated for the different polarized states of the incident light with a 4×4 transfer matrix method

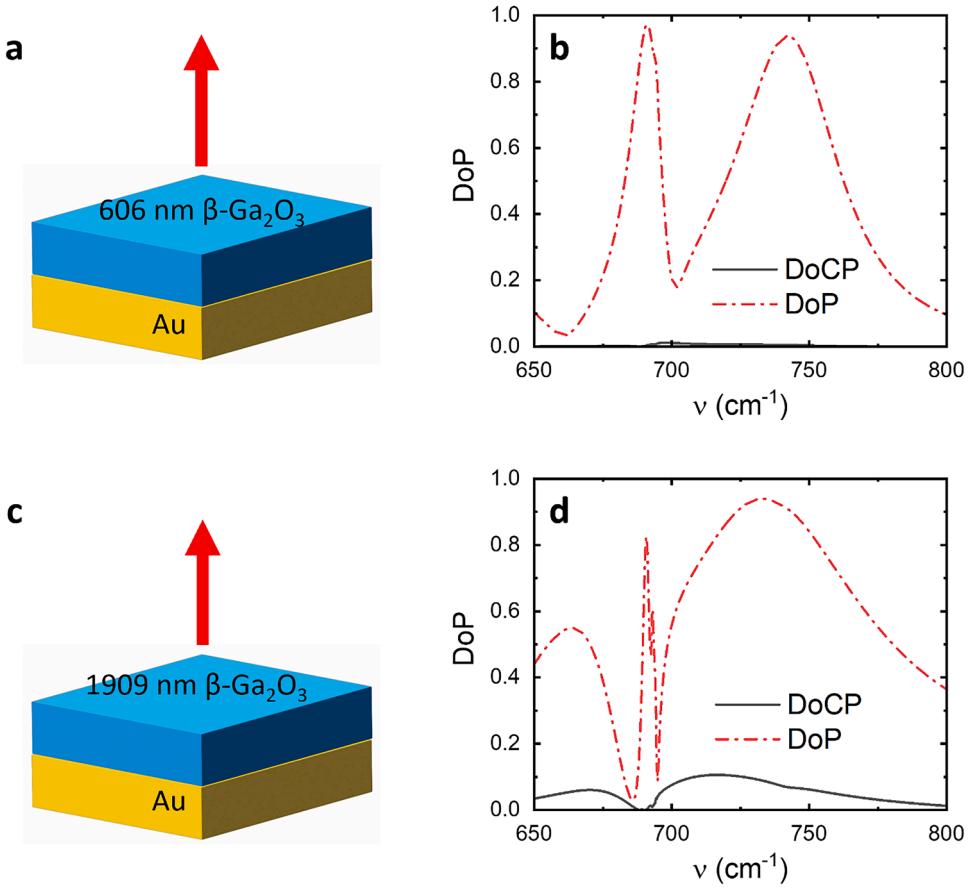

Fig. 2. (a) Schematic of a single β-Ga_2O_3 layer exhibiting optimized DoP at ν=691 cm^{-1}; (b) DoP and DoCP as a function of the frequency for the system sketched in (a); (c) Schematic of a single β-Ga_2O_3 layer exhibiting optimized DoP at ν=737 cm^{-1}; (d) DoP and DoCP as a function of the frequency for the system sketched in (c).

[41]. The DoP and the DoCP are then defined as:

$$\mathrm{DoP} = \frac{\sqrt{S_1^2 + S_2^2 + S_3^2}}{S_0} \tag{3}$$

$$\mathrm{DoCP} = \frac{|S_3|}{S_0} \tag{4}$$

Being both DoP and DoCP limited in the range [0,1] and DoCP≤DoP. DoP=1 stands for perfectly polarized light, thus DoCP=1 corresponds to perfectly circularly polarized light.

Our approach is based on the combination of two layers on top of gold substrate. The bottom layer acts as an emitter while the second acts as a quarter-wave plate. Both layers are required to be strongly anisotropic, however, the emitting layer should provide high emission/absorption efficiency for only one polarization component while the upper one should be as transparent as possible with a strong anisotropic real part of the refractive index. A particle swarm optimization is used as the search algorithm for the optimal parameters including the thicknesses of the MoO_3 layer (d_1), the Ga_2O_3 layer (d_2), and the twist angle between the two layers (α). In order to reduce the number of optimization parameters and to avoid local minimum solutions for the two-layer system the particle swarm algorithm is performed in two separate steps. At first, we focus on the single bottom layer on gold. This way we find the layer thickness d_2 and emission wavelength for maximized DOP. Then we optimize the thickness and the relative orientation of the second (upper) layer to obtain maximum DoCP. We focus on the fact that this two-step optimization is performed to reduce the number of simultaneous sweeping parameters but it does not affect the accuracy of numerical results. Indeed, the adopted 4 × 4 transfer matrix model takes into account for multiple reflections. A complete single-step full sweep could lead to improved performances at a slightly shifted emission line. Nevertheless, we expect that this shift, typically related to multiple reflections, could play a relevant role in multilayer stacks or high-Q cavities, here we only focus on the double-layer scheme.

3. Materials optical properties

We study both α-MoO_3 and β-Ga_2O_3 optical properties in the mid-IR with the aim of identifying the frequency ranges where they can be efficiently combined. To begin with, we focus our study on the thermal radiation emitted along the direction normal to the surface. Thus, if we consider the *x*-*y* plane as the surface plane, the emission direction is toward the *z*-axis. We also select the orientation of the crystals so that *x*- and *y*- axes coincide with the *x*'- and *y*'- crystal axes. In this case, we are interested in the in-plane values of the dielectric permittivities. In Fig. 1 (a,b), the imaginary part of *xx*, *yy* and *xy* components of the relative permittivity tensor of α-MoO_3 and β-Ga_2O_3 are plotted as a function of the frequency [23,42]. The imaginary part of the dielectric function is related to absorption/emission. For α-MoO_3, there are two main peaks at 550 cm^{-1} and 820 cm^{-1} due to optical phonons while for β-Ga_2O_3, there are three main bands centered around 570 cm^{-1}, 690 cm^{-1} and 740 cm^{-1}, respectively. As previously mentioned, in our emitter/waveplate approach we want to avoid overlaps in the emission bands in order to clearly distinguish the role of the emitter from the role of the waveplate. For this reason, we exclude from further investigation the lower frequencies (570 cm^{-1} and 550 cm^{-1}). In Fig. 1(c), the real part of the refractive index components n_x and n_y α-MoO_3 and their $\Delta n = n_x - n_y$ are shown. The real part of the dielectric function components of β-Ga_2O_3 are shown in Fig. 1(d). We note that α-MoO_3 has a wide band (from 600 cm^{-1} to 750 cm^{-1}) of high and almost constant anisotropy which makes

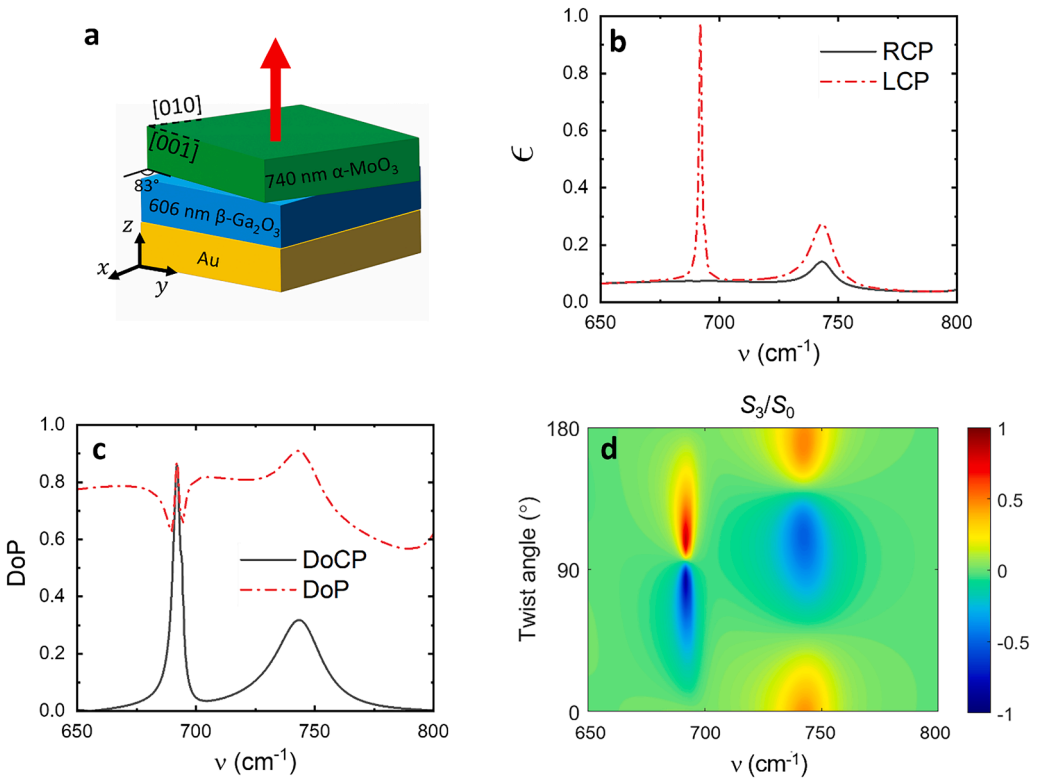

Fig. 3. (a) Schematic of twisted bi-layer structure designed for ν=691 cm^{-1}, obtained by adding a α-MoO_3 layer on top of the β-Ga_2O_3 layer; (b) circularly polarized emissivity and (c) degree of polarization of the twisted bi-layer structure; (d) S_3/S_0 as a function of the twist angle and of the frequency. We note that by proper tuning of the twist angle, it is possible to switch from LCP to RCP emission at ν=691 cm^{-1}.

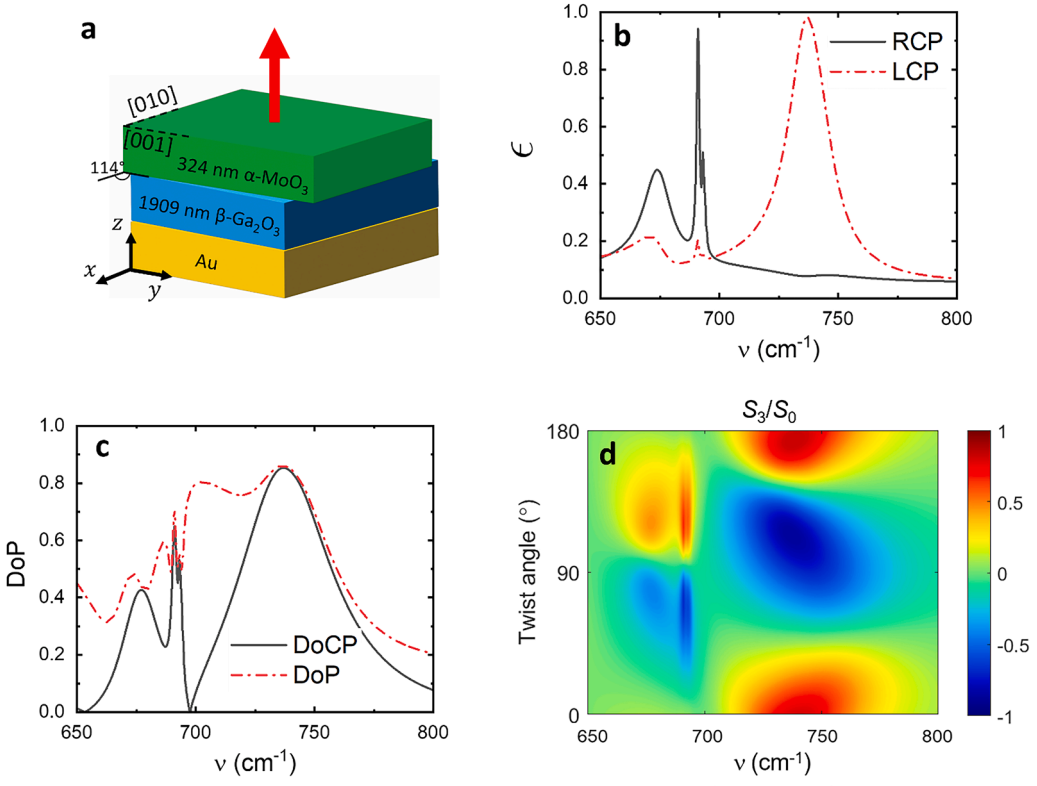

Fig. 4. (a) Schematic of twisted bi-layer structure designed for ν=737 cm^{-1}, obtained by adding a α-MoO_3 layer on top of the β-Ga_2O_3 layer; (b) circularly polarized emissivity and (c) degree of polarization of the twisted bi-layer structure; (d) S_3/S_0 as a function of the twist angle and of the frequency. We note that by proper tuning of the twist angle it is possible to switch from LCP to RCP emission at ν=737 cm^{-1}.

it very suitable to be used as a waveplate. Thus we focus our attention on the design of an efficient β-Ga_2O_3 emitting layer around 690 cm^{-1} and 740 cm^{-1} with a high DoP combined with a properly tilted and sized α-MoO_3 layer acting as waveplate to obtain a tailored thermal source with optimized DoCP.

4. Results and discussion

We employed particle swarm optimization (PSO), a search algorithm that finds optimal solutions by iteratively trying to improve candidate solutions, and finally obtained structures with the highest circular emission at specific frequencies. The independent parameters needed according to the proposed two-layer scheme are the thicknesses of the MoO_3 layer (d_1), of the Ga_2O_3 layer (d_2), and the twist angle between the two layers (α). These parameters are grouped into a vector, denoted as $\mathbf{r}$, which serves as a particle. An initial population of N random particles is generated, and the loss function of each particle is calculated. Subsequently, the particles undergo iterative exploration of the parameter space to minimize the loss function until the predetermined iteration number is reached. More details of the particle swarm optimization algorithm can be found in the reference [43]. However, in order to reduce the number of optimization parameters and to avoid local minimum solutions for the two-layer system the particle swarm algorithm is performed in two separate steps. The first optimization is performed on a single β-Ga_2O_3 layer on gold substrate looking for maximum DOP. We set as the loss function $y(\mathbf{r}) = 1 - \text{DoP}$ (thus $\boldsymbol{r} = [d_2]$). We found two schemes, named scheme A and scheme B, corresponding to maximized DoP at two different frequencies: 691 cm^{-1} and 737 cm^{-1} respectively. In the first scheme, sketched in Fig. 2a, we note that a $d_{2,A} = 606$ nm thick β-Ga_2O_3 layer has a maximum relative emissivity for a *p*-polarized field at 691 cm^{-1} corresponding to a DoP of about 0.97 and zero DoCP (Fig. 2b). On the other hand, the second proposed scheme, sketched in Fig. 2c is based on a thicker Ga_2O_3 layer ($d_{2,B} = 1909$ nm) showing a maximum DoP=0.93 at ν=737 cm^{-1}. The main difference with respect to the previous case is that the initial DoCP is now about 0.1 (Fig. 2d). Thus the emitted radiation from the single Ga_2O_3 layer is elliptical.

Then we added a MoO_3 cap layer to both schemes and applied a second PSO varying the thickness d_1 and the relative orientation α with respect to the bottom layer. For the first scheme an initial population of $N = 30$ particles (with $\mathbf{r}_A = [d_1, d_{2,A}, \alpha]$ and random d_1 and α) is generated. The loss function of each particle, defined as $y(\mathbf{r}) = 1 - \text{DoCP}$, is calculated and a predetermined iteration number of 150 is chosen. We found an optimal condition corresponding to a DoCP=0.87 at 691 cm^{-1} when a $d_{1,A} = 740$ nm α-MoO_3 layer, tilted by an angle $\alpha_A = 83°$ in the *x*-*y* plane with respect to the *x*'*y*' axes of the β-Ga_2O_3 layer is considered (sketch of Fig. 3a). All the results have been obtained with the indirect method, (i.e., calculating the absorptivity and applying Kirchhoff's law) and validated by the direct method based on fluctuation electrodynamics [38]. Fig. 3b shows a high peak of almost left circularly polarized (LCP) emission at ν=691 cm^{-1}. The corresponding DoP and DoCP are reported in Fig. 3c. We note that DoP=DoCP=0.87 at nearly the same frequency (see Fig. 3c). Finally, we report in Fig. 3d the value of S_3/S_0 as a function of the twist angle between the two layers and of the frequency. Its modulus is the DOCP, however, its sign determines the Right (if positive) or Left (if negative) circular polarization. The reported map clearly shows that at ν=691 cm^{-1} it is possible to switch from almost perfect (DoCP=0.87) RCP to LCP by properly tuning the twist angle.

An analogous approach has been applied for the scheme B. Optimized performances are achieved for the second scheme by adding a $d_{1,B} = 324$ nm thick layer of α-MoO_3 as sketched in Fig. 4a, rotated in the *x*-*y* plane by α_B=114° with respect to the *x*'*y*' axes of the β-Ga_2O_3 layer. We note that in this case, we obtain a resulting DoP = DoCP = 0.85 (Fig. 4c) and the thermal emitted radiation at 737 cm^{-1} is mostly left circularly polarized (Fig. 4b). However, right-hand circular polarization at 737 cm^{-1} can be obtained similarly to the previous scheme, by varying the twist angle of the MoO_3 layer as shown in Fig. 4d.

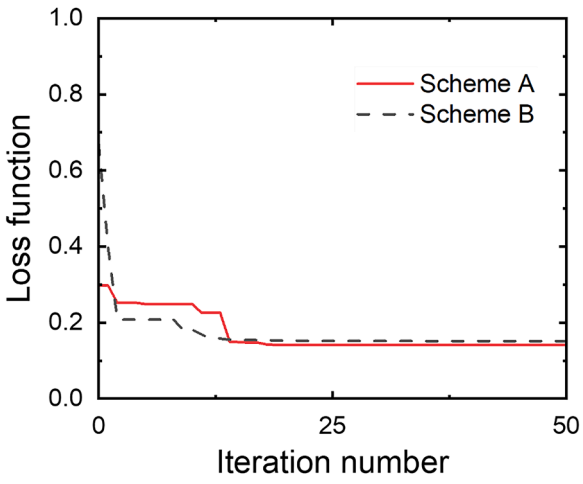

Fig. 5. Convergence plot of the particle swarm optimization process for scheme A (as illustrated in Fig. 3) and scheme B (as illustrated in Fig. 4).

Fig. 5 illustrates the final optimization process of scheme A (Fig. 3) and scheme B (Fig. 4), denoted by the red solid line and black dashed line, respectively. The minimum obtained loss function among $N = 30$ particles is plotted as a function of iteration number. It can be observed that after the 25th iteration, the optimization reaches a converged value. Scheme A has a loss function of 0.13, corresponding to a DoCP of 0.87, while scheme B has a loss function of 0.15, indicating a DoCP of 0.85. We finally explore the robustness of the proposed schemes by varying the emission angle i.e. the azimuth angle (ϕ) and zenith angle (θ)) to show that the results are maintained over a large angular range for both schemes (Fig. 6a and 6b respectively).

Further evidence of the robustness of the bi-layer approach is reported in Fig. 6. We performed single parameters sweep (on Ga_2O_3layer and on MoO_3 layer thickness) around the optimal conditions for scheme A (Fig. 7a,b) and scheme B (Fig. 7c,d). We show that high degree of circular polarization is maintained over a large range of the thickness of the layers corresponding to hundreds of nm. We note that scheme 1 allows for a narrow band emission with a good tunability of 5 cm^{-1}, varying the thickness of the Ga_2O_3 layer and maintaining a DoCP higher than 0.7. On the other hand, scheme B emits on a larger bandwidth and it is extremely robust with respect to tolerances on the layer's thickness.

5. Conclusion

We proposed a lithography-free method based on a double-twisted layer scheme to obtain circularly polarized thermal radiation in the mid-IR, at two specific frequencies related to β-Ga_2O_3 optical phonons excitation. The almost linearly polarized emission from the single slab is converted into circular polarization by adding a properly sized and tilted α-MoO_3 layer acting as a quarter-wavelength plate. In both cases, we take advantage of the strong natural anisotropy related to the low symmetry class of the investigated materials without the need for further processing techniques. The achieved degree of circular polarization is higher than 0.85 for the two proposed schemes and it is maintained over a broad range of angles of emission. We believe that this approach could lead to the development of low-cost, integrated thermal sources of circularly polarized light for IR sensing applications.

CRediT authorship contribution statement

Marco Centini: Conceptualization, Data curation, Formal analysis, Investigation, Methodology, Software, Writing – original draft, Writing – review & editing. **Chiyu Yang:** Conceptualization, Data curation, Formal analysis, Methodology, Software, Writing – original draft, Writing – review & editing. **Maria Cristina Larciprete:** Formal analysis,

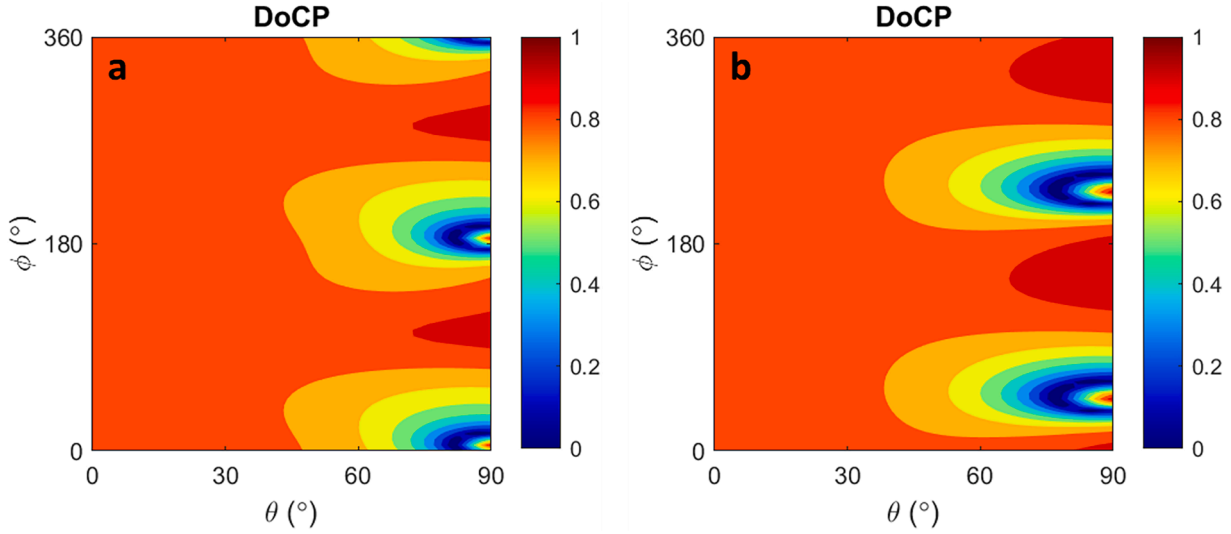

Fig. 6. DoCP of thermal radiation emitted (a) at ν=691 cm^{-1} for the structure sketched in Fig. 3a and (b) at ν=737 cm^{-1} for the structure sketched in Fig. 4a as a function of angle (ϕ) and zenith angle (θ).

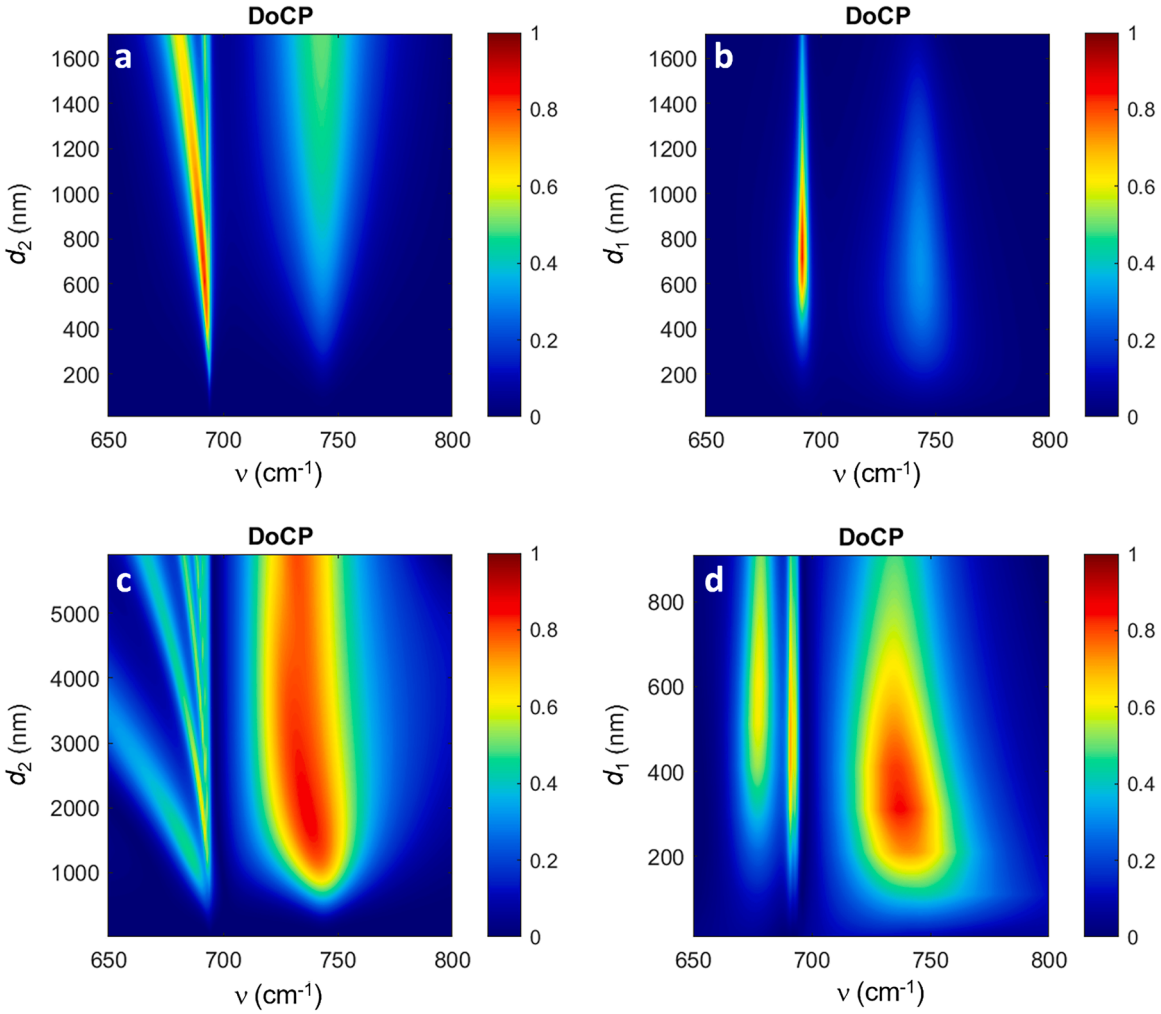

Fig. 7. DoCP as a function of the frequency and the (a) β−Ga2O3 layer thickness, (b) α−MoO3 layer thickness for scheme A. DoCP as a function of the frequency and the (c) β−Ga2O3 layer thickness, (d) α−MoO3 layer thickness for scheme B.

Investigation, Visualization, Writing – original draft, Writing – review & editing. **Mauro Antezza:** Conceptualization, Supervision, Writing – original draft, Writing – review & editing. **Zhuomin M. Zhang:** Formal analysis, Investigation, Methodology, Supervision, Visualization, Writing – original draft, Writing – review & editing.

Declaration of competing interest

The authors declare that they have no known competing financial interests or personal relationships that could have appeared to influence the work reported in this paper.

Data availability

Data will be made available on request.

Acknowledgements

M.A. thanks the SAPIENZA University of Rome and the Department of Basic and Applied Sciences for Engineering for hospitality during his stay in Rome under the visiting professor program, where this work has been initiated. M.C, M.C.L, M.A. and Z.M.Z. acknowledge the KITP program 'Emerging Regimes and Implications of Quantum and Thermal Fluctuational Electrodynamics' 2022, where part of this work has been done. This research was supported in part by the National Science Foundation under Grant No. PHY-1748958. C.Y. was supported by the National Science Foundation (CBET-2029892).

References

[1] Hodgkinson J, Tatam RP. Optical gas sensing: a review. Meas Sci Technol 2013;24(1):012004.
[2] Furstenberg R, Kendziora CA, Stepnowski J, Stepnowski SV, Rake M, Papantonakis MR, Nguyen V, Hubler GK, McGill RA. Stand-off detection of trace explosives via resonant infrared photothermal imaging. Appl Phys Lett 2008;93(22):224103.
[3] Wood MF, Côté D, Vitkin IA. Combined optical intensity and polarization methodology for analyte concentration determination in simulated optically clear and turbid biological media. J Biomed Opt 2008;13(4):044037.
[4] F. Snik, J. Craven-Jones, M. Escuti, S. Fineschi, D. Har-rington, A.D. Martino, D. Mawet, J. Riedi, and J.S. Tyo, in Polarization: measurement, analysis, and re-mote sensing XI, Vol. 9099, D. B. Chenault and D. H. Goldstein, International society for optics and photonics (SPIE, 2014) p. 90990.
[5] Chen Y, Francescato Y, Caldwell JD, Giannini V, Maß TWW, Glembocki OJ, Bezares FJ, Taubner T, Kasica R, Hong M, Maier SA. Spectral tuning of localized surface phonon polariton resonators for low-loss mid-IR applications. ACS Photonics 2014;1(8):718–24.
[6] Caldwell JD, et al. Low-loss, infrared and terahertz nanophotonics using surface phonon polaritons. Nanophotonics 2015;4:44–68.
[7] Zhang ZM. Nano/microscale heat transfer. 2nd ed. Springer; 2020.
[8] Greffet J-J, Carminati R, Joulain K, Mulet J-P, Mainguy S, Chen Y. Coherent emission of light by thermal sources. Nature 2002;416(6876):61–4.
[9] Larciprete MC, Centini M, Voti RLi, Sibilia C. Selective and tunable thermal emission in metamaterials composed of oriented polar inclusions. J Opt Soc Am B 2017;34(7):1459–64.
[10] Lochbaum A, Fedoryshyn Y, Dorodnyy A, Koch U, Hafner C, Leuthold J. On-chip narrowband thermal emitter for mid-IR optical gas sensing. ACS Photonics 2017;4(6):1371–80.
[11] Overvig AC, Mann SA, Alù A. Thermal metasurfaces: complete emission control by combining local and nonlocal light-matter interactions. Phys Rev X 2021;11:021050.
[12] Centini M, Larciprete MC, Voti RLi, Bertolotti M, Sibilia C, Antezza M. Hybrid thermal Yagi-Uda nanoantennas for directional and narrow band long-wavelength IR radiation sources. Opt Express 2020;28:19334–48.
[13] Li C, Krachmalnicoff V, Bouchon P, Jaeck J, Bardou N, Haïdar R, De Wilde Y. Near-field and far-field thermal emission of an individual patch nanoantenna. Phys Rev Lett 2018;121(24):243901.
[14] Poddubny A, Iorsh I, Belov P, Kivshar Y. Hyperbolic metamaterials. Nat Photon 2013;7:948.
[15] Lee M, Lee E, So S, Byun S, Son J, Ge B, Lee H, Park HS, Shim W, Pee JH, Min B, Cho S-P, Shi Z, Noh TW, Rho J, Kim J-Y, Chung I. Bulk metamaterials exhibiting chemically tunable hyperbolic responses. J Am Chem Soc 2021;143(49):20725–34.
[16] Wu F, Wu X, Xiao S, Liu G, Li H. Broadband wide-angle multilayer absorber based on a broadband omnidirectional optical Tamm state. Opt Express 2021;29(15):23976–87.
[17] Wu F, Chen M, Xiao S. Wide-angle polarization selectivity based on anomalous defect mode in photonic crystal containing hyperbolic metamaterials. Opt Lett 2022;47(9):2153–6.
[18] Campione S, Marquier F, Hugonin J-P, Ellis AR, Klem JF, Sinclair MB, Luk TS. Directional and monochromatic thermal emitter from epsilon-near-zero conditions in semiconductor hyperbolic metamaterials. Sci Rep 2016;6(1):34746.
[19] Simovski C, Maslovski S, Nefedov I, Tretyakov S. Optimization of radiative heat transfer in hyperbolic metamaterials for thermophotovoltaic applications. Opt Express 2013;21(12):14988–5013.
[20] Zhang Q, Hu G, Ma W, Li P, Krasnok A, Hillenbrand R, Alù A, Qiu C-W. Interface nano-optics with van der Waals polaritons. Nature 2021;597(7875):187–95.
[21] Caldwell JD, Aharonovich I, Cassabois G, et al. Photonics with hexagonal boron nitride. Nat Rev Mater 2019;4:552–67.
[22] Álvarez-Pérez G, Folland TG, Errea I, Taboada-Gutiérrez J, Duan J, Martín-Sánchez J, Tresguerres-Mata AIF, Matson JR, Bylinkin A, He M, Ma W, Bao Q, Martín JI, Caldwell JD, Nikitin AY, Alonso-González P. Infrared permittivity of the biaxial van der waals semiconductor α-MoO3 from near- and far-field correlative studies. Adv Mater 2020;32(29):1908176.
[23] Zheng Z, Xu N, Oscurato SL, Tamagnone M, Sun F, Jiang Y, Ke Y, Chen J, Huang W, Wilson WL, Ambrosio A, Deng S, Chen H. A mid-infrared biaxial hyperbolic van der Waals crystal. Sci Adv 2019;5(5):eaav8690.
[24] Abedini Dereshgi S, Folland TG, Murthy AA, Song X, Tanriover I, Dravid VP, Caldwell JD, Aydin K. Lithography-free IR polarization converters via orthogonal in-plane phonons in α-MoO3 flakes. Nat Commun 2020;11(1):5771.
[25] Abedini Dereshgi S, Larciprete MC, Centini M, Murthy AA, Tang K, Wu J, Dravid VP, Aydin K. Tuning of optical phonons in α-MoO3–VO2 multilayers. ACS Appl Mater Interfaces 2021;13(41):48981–7.
[26] Deng G, Abedini Dereshgi S, Song X, Wei C, Aydin K. Phonon-polariton assisted broadband resonant absorption in anisotropic α-phase Mo O3" nanostructures. Phys Rev B 2020;102(3):035408.
[27] Cristina Larciprete Maria, Dereshgi Sina Abedini, Centini Marco, Aydin Koray. Tuning and hybridization of surface phonon polaritons in α-MoO3 based metamaterials. Opt Express 2022;30:12788–96.
[28] Hu G, Ou Q, Si G, Wu Y, Wu J, Dai Z, Krasnok A, Mazor Y, Zhang Q, Bao Q, Qiu C-W, Alù A. Topological polaritons and photonic magic angles in twisted α-MoO3 bilayers. Nature 2020;582(7811):209–13.
[29] Wu X, Fu C, Zhang ZM. Near-field radiative heat transfer between two α-MoO3 biaxial crystals. J Heat Transfer 2020;142(7):072802.
[30] Wu B-Y, et al. Strong chirality in twisted bilayer α-MoO3. Chinese Phys B 2022;31:044101.
[31] Wu B-Y, Wang M, Wu F, Wu X. Strong extrinsic chirality in biaxial hyperbolic material α-MoO3 with in-plane anisotropy. Appl Opt 2021;60:4599–605.
[32] Liu P, Zhou L, Tang J, Wu B-Y, Liu H, Wu X. Spinning thermal radiation from twisted two different anisotropic materials. Opt Express 2022;30:32722–30.
[33] Ma W, Alonso-González P, Li S, Nikitin AY, Yuan J, Martín-Sánchez J, Taboada-Gutiérrez J, et al. In-plane anisotropic and ultra-low-loss polaritons in a natural van der Waals crystal. Nature 2018;562(7728):557–62.
[34] Urban FK, Barton D, Schubert M. Numerical ellipsometry: a method for selecting a near-minimal infrared measurement set for β-gallium oxide. J Vacuum Sci Technol 2021;39(5):052801.
[35] Zhao M, Tong R, Chen X, Ma T, Dai J, Lian J, Ye J. Ellipsometric determination of anisotropic optical constants of single phase Ga2O3 thin films in its orthorhombic and monoclinic phases. Opt Mater 2020;102:109807.
[36] Passler NC, Ni X, Hu G, et al. Hyperbolic shear polaritons in low-symmetry crystals. Nature 2022;602:595–600.
[37] Zhou C-L, Tang G, Zhang Y, Antezza M, Yi H-L. Radiative heat transfer in a low-symmetry Bravais crystal. Phys Rev B 2022;106:155404.
[38] Yang C, Cai W, Zhang ZM. Polarimetric analysis of thermal emission from both reciprocal and nonreciprocal materials using fluctuation electrodynamics. Phys Rev B 2022;106:245407.
[39] Olmon RL, Slovick B, Johnson TW, Shelton D, Oh S-H, Boreman GD, Raschke MB. Optical dielectric function of gold. Phys Rev B 2012;86:235147.
[40] Marquier F, Arnold C, Laroche M, Greffet JJ, Chen Y. Degree of polarization of thermal light emitted by gratings supporting surface waves. Opt Express 2008;16:5305.
[41] Passler NC, Paarmann &A. Generalized 4 × 4 matrix formalism for light propagation in anisotropic stratified media: study of surface phonon polaritons in polar dielectric heterostructures. J Opt Soc Am B 2017;34:2128–39.
[42] Schubert M, Korlacki R, Knight S, Hofmann T, Schöche S, et al. Anisotropy, phonon modes, and free charge carrier parameters in monoclinic β-gallium oxide single crystals. Phys Rev B 2016;93:125209.
[43] Kennedy J, Eberhart R. Particle swarm optimization. In: Proceedings of ICNN'95-international conference on neural networks. ieee; 1995. p. 1942–8.